Nonlinear dynamics of driven relativistic electron plasma waves

W. P. Leemans,* C. Joshi, W. B. Mori, and C. E. Clayton
Electrical Engineering Department, University of California, Los Angeles, Los Angeles, California 90024

T. W. Johnston
Institut National de Recherche Scientifique–Energie Case Postale 1020, Varennes Quebec, Canada J3X 1S2
(Received 20 December 1991; revised manuscript received 4 May 1992)

We have examined the nonlinear dynamics associated with beat-wave $(\Delta\omega,\Delta k)$ generation of long-wavelength plasma waves $(\Delta k \leq \omega_p/c)$ in the presence of a strong $(\delta n/n - 0.15$ to $0.75)$ short-wavelength density ripple $[k_i - (5$ to $130)\ \Delta k]$ using the relativistic Lagrangian-oscillator model. Two cases are considered: time-varying detuning ratio $(\omega_p/\Delta\omega)$ and time-varying laser intensity I. In the absence of the plasma ripple, it is found that the Lagrangian-oscillator motion contains half-harmonic components in an Arnold tonguelike parameter space $(\omega_p/\Delta\omega, v_{\rm osc}/c)$ centered around $\omega_p/\Delta\omega \approx 0.5$. The effect of the ripple is twofold: (a) It lowers the minimum driver strength needed to access the half-harmonic parameter region around $\omega_p/\Delta\omega \approx 0.5$, and (b) it makes a second parameter region available, centered around $\omega_p/\Delta\omega \approx 2.0$. Although the Lagrangian model exhibits further period doubling followed by a transition to chaos when a time-varying laser intensity is used, wave breaking sets in after the first bifurcation, thereby limiting the validity of the model. The origin of the first period doubling, however, is found to be linked to the stability of an equivalent Mathieu equation to $\frac{1}{2}$ subharmonic resonances. Finally, a particle-in-cell-code simulation shows spatial wave-number peaks displaced by $\Delta k/2$ on both sides of the driver frequencies, giving support to the idea that the first bifurcation behavior may be observable in an experiment.

PACS number(s): 52.40.Nk, 52.60.+h, 52.35.−g

I. INTRODUCTION

The complex dynamical behavior of driven nonlinear oscillators has received much interest in the past decade. Physical systems modeled through nonlinear oscillators have been identified in many areas including fluid mechanics, physical chemistry, laser physics, nonlinear optics, and electronics. Such nonlinear oscillators exhibit phenomena such as bistability, hysteresis, and the occurrence of subharmonics followed by a transition to chaos. The behavior of driven relativistic large-amplitude electron plasma waves can be described by model equations essentially reducible to a nonlinear oscillator equation which therefore exhibits the aforementioned phenomena. Through collinear optical mixing in a plasma [1] such a wave can be easily excited. Thus it is possible to study these fundamental phenomena experimentally, allowing one to explore the relationship between temporal and spatial subharmonics and the transition to chaos in a plasma system.

In collinear optical mixing two laser beams with slightly different frequencies, ω_1 and ω_2, are injected into a plasma. If the difference frequency $\Delta\omega(=\omega_1-\omega_2)$ is approximately equal to the plasma frequency, the ponderomotive force associated with the laser light will resonantly excite a longitudinal plasma oscillation. Energy and momentum conservation require

$$\omega_1-\omega_2=\omega_p\ , \tag{1}$$

$$k_1 \pm k_2 = k_p\ , \tag{2}$$

where the $\pm$ stands for co- or counterpropogating laser beams. The phase velocity of the plasma wave in the case of copropagating beams equals the mean group velocity of the light waves, which for an underdense plasma is almost the speed of light in a vacuum. It was suggested by Tajima and Dawson to use these high-phase velocity, large-amplitude plasma waves for particle acceleration, known as the plasma beat-wave accelerator [2].

In order to achieve considerable acceleration gradients (i.e., large electric fields) inside the plasma large laser intensities are required, and one arranges the experiment so that the plasma density gives a plasma frequency equal to the beat frequency, i.e., $\omega_p/\Delta\omega \approx 1$. The large laser intensity can lead to the phenomenon of relativistic detuning of the plasma frequency [1] and is usually time varying. In experiments the actual obtained plasma density can differ significantly from the resonant density and may also vary in time. Furthermore, in the process of building up the large-amplitude plasma wave, competing instabilities such as stimulated Raman scattering (SRS) and/or stimulated Compton scattering (SCS) and stimulated Brillouin scattering (SBS) will scatter laser energy out of the plasma and create low-phase-velocity short-wavelength electron plasma waves and ion waves [3]. These waves represent in effect a spatial and temporal modulation of the plasma dielectric constant.

In this paper we study through numerical modeling the nonlinear dynamics associated with the generation of a plasma beat wave in such a spatially modulated plasma under temporally varying conditions. In Sec. II we delineate the problem associated with varying the plasma

frequency in time and derive the well-known relativistic Lagrangian oscillator model [4] with the addition of a rippled component to the plasma density. The effective damping in the equation of motion of the fluid momentum will contain a contribution of the ionization rate for the case of a temporally varying plasma density.

The obtained equations are then solved numerically in Sec. III giving the following results: The plasma wave exhibits hysteresis when the plasma density (laser intensity) is varied in time, for a given damping rate, wavelength, and amplitude of the plasma ripple, and a laser intensity (plasma density). Furthermore, when the laser intensity is varied in time, regions in parameter space are found where the motion of the fluid element shows period doubling followed by chaotic motion [5] or where an incomplete period-doubling tree [6] is observed. However, reconstructing the waveform in the laboratory frame we find that wavebreaking occurs before the second bifucation thereby limiting the validity of our model. The physical origin of the first bifurcation is analyzed by applying a perturbation technique to an equivalent generalized Mathieu equation.

In Sec. IV results are shown from the fully relativistic, electromagnetic, particle-in-cell code WAVE [7] which has been used to verify the validity of the analytic model. It includes all the effects competing with the buildup of a large amplitude plasma wave in one dimension. We conclude with a summary of the obtained results.

II. LAGRANGIAN MODEL OF RELATIVISTIC PLASMA WAVES

A. Why a Lagrangian model?

The nonlinear features of the plasma wave can be classified into two categories: bistability, with the associated hysteresis effect, and the existence of subharmonics with the possibility of a transition to chaos. Bistability and hysteresis were inherently present in the work of Tang *et al.* [4] but were discussed more explicitly by Ma and Xu [8] within the slowly varying envelope approximation. They studied the case where the time-varying plasma frequency is very close to the resonance frequency $\Delta\omega$, for $\alpha_1\alpha_2$ much less than one where α_i is the quiver velocity of the electron in the laser field normalized to the speed of light $v_{\rm osc}/c$. The damping in their model is dominated by collisional effects but they neglected any velocity dependence of the collision frequency. Furthermore, the assumption that the fluid element displacement is modeled by

$$\xi(\tau,w_0)=\epsilon(\tau)\sin[\tau-w_0+\Phi(\tau)] , \tag{3}$$

where ϵ and Φ are the slowly varying amplitude and phase, respectively, precludes the authors from observing subharmonics in the motion of the fluid elements.

The possibility of chaotic behavior of the plasma wave for large driver strengths has been discussed by Mendonça [9]. In this paper the analogy was used between the equation of motion of the longitudinal electric field, derived under the weakly relativistic approximation, and the Duffing equation [10]. The weakly relativistic approximation is valid when α_i is much less than 1 and the amplitude of the plasma wave satisfies the condition $n_1/n_0 \ll 1$, where n_1 is amplitude of the density modulation and n_0 is the background plasma density. The Duffing equation models the motion of a nonrelativistic particle in an anharmonic potential. It has been shown [11] that chaotic motion occurs for displacements which brings the oscillator close to the turning points of the potential.

First, as pointed out by Mori [12] and by McKinstrie and Forslund [13], Mendonça erred in the sign of the frequency detuning of the plasma frequency in the equation of motion of the longitudinal electric field. When deriving the equivalent potential from the restoring force terms in the equation of motion, this leads to the wrong shape of the anharmonic potential. Second, even for the correct shape of the potential we found that, analogous to the Duffing oscillator, chaotic motion occurs for displacements that bring the oscillator close to the turning points of the potential. However, when treating the relativistic terms exactly one arrives at a shape of the associated potential well which does not have any turning points. Indeed, in a one-dimensional Lagrangian frame it is straightforward to show that the equation of motion in the absence of damping for the momentum of relativistic plasma waves is given in its simplest form by

$$\frac{d^2p}{dt^2}+\omega_p^2\frac{p}{\sqrt{1+p^2}}=\frac{d}{dt}F_{NL} , \tag{4}$$

where p is the momentum of the fluid element and F_{NL} is the ponderomotive force. The restoring force can now be derived from a potential

$$V(p)=\sqrt{1+p^2}-1 . \tag{5}$$

In Fig. 1 we show the exact potential as given by Eq. (5) and its Taylor expansion up to second order, which is equivalent to the aharmonic potential in the Duffing model. As can be seen from Fig. 1, the two potentials start differing significantly in shape beyond $|p|=1$ and the use of the Taylor expansion for the potential is not justified for the large-momentum regime for the following reasons. While the exact potential has only one stable equilibrium point and the radius of curvature of the po-

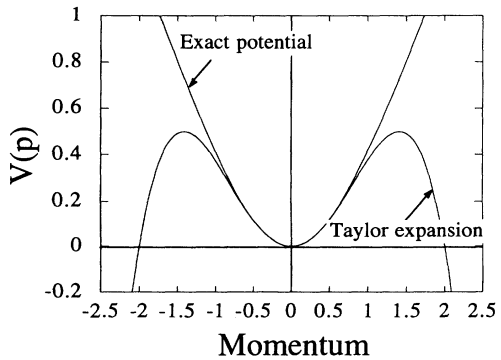

FIG. 1. Plot of potential $V(p)=\sqrt{1+p^2}-1$ and its Taylor expansion $p^2/2-p^4/8$.

tential never changes sign, its Taylor expansion has one stable and two unstable equilibrium points and clearly, the radius of curvature of this potential changes sign.

From nonlinear dynamics it is well known that the existence of unstable equilibrium points changes the behavior of any system in a fundamental way. In particular for the Duffing oscillator it is found that (a) it exhibits hysteresis and period doubling only for driver strengths that bring the oscillator close to these unstable points; (b) when the amplitude exceeds momentarily the turning-point limit, the oscillator is unstable and undergoes a jump to the lower amplitude branch or continues to roll down the potential towards infinity. From this we conclude that the rich nonlinear behavior (i.e., period-doubling route to chaos and bistability) exhibited by the model equation of the longitudinal electric field as obtained under the weakly relativistic approximation, is an artefact of this approximation [14].

However, it is well understood that the Duffing oscillator undergoes period doubling and shows hysteresis when the particle moves in an asymmetric potential well. In practice such a situation can arise without the excursion of the fluid element becoming unreasonably large when the wave is excited in a plasma whose density is rippled. The background plasma can be rippled, for example, due to the presence of a SRS and/or SCS-generated slow-phase-velocity electron plasma wave or due to a SBS-generated ion wave.

B. Fluid equations for ionizing plasma

Since in the beat excitation of relativistic plasma waves the amplitude of the longitudinal electric field is critically dependent on the ratio $\omega_p/\Delta\omega$, it is necessary to study the effect of detuning ($\Delta\omega \neq \omega_p$) caused by a time-dependent plasma density [15]. The main phenomenon leading to a time dependence of the bulk plasma density in the focal volume of the laser beam on a time scale relevant for the beat excitation is laser-induced ionization. Ponderomotive and/or thermal self-focussing [16], which decreases the plasma density, occurs on a time scale set by the ions and will not be included in our analytic model.

This ionizing plasma can be modelled with the following two approaches. In the first approach one treats each newly added amount of electrons and ions as a new species in the plasma. The new species starts out at rest and will move under the influence of the electromagnetic fields present inside the plasma. It is then necessary to solve a system of N-coupled second-order nonlinear differential equations, where N is the number of groups of plasma "species" one wishes to follow, making a rigorous analytic treatment of this problem not tractable. The second approach involves making the following approximation: We model the plasma using a one-particle distribution function [17]. The momentum associated with an infinitely small fluid element is obtained by adding up the momentum vectors of each individual particle. So, when new particles, which are initially at rest, are added to a particular fluid element, its total density increases while its momentum is reduced.

The functional form describing the rate at which new plasma is being produced depends on the involved ionization process. Consider therefore a beat-wave excitation experiment using a high-intensity ($I > 10^{14}\mathrm{W/cm^2}$) CO_2 laser [18]. For such a long-wavelength, high-intensity laser the Keldysh parameter [19] is much smaller than 1. Tunneling ionization is then the dominant process in the plasma formation. Since the newly born electrons start out at rest the source of the plasma can be modeled as

$$S(\mathbf{r},\mathbf{p},t)=\lambda(t)[N_0-n(\mathbf{r},t)]\delta(\mathbf{p}) , \tag{6}$$

where $\lambda(t)$ is the time-dependent ionization rate, $\mathbf{r}$ and $\mathbf{p}$ are, respectively, the position and momentum vectors of the fluid element, t is the time, N_0 and $n(\mathbf{r},t)$ are the neutral gas density and plasma density, respectively. The Dirac function in the source term implies that the electrons are born at rest.

The fluid equations are obtained by taking moments of the Vlasov equation with this source term. The details of the derivation are given in the Appendix. The resulting equation of continuity is then

$$\frac{\partial n(\mathbf{r},t)}{\partial t}+\frac{\partial}{\partial \mathbf{r}}\cdot\left[n(\mathbf{r},t)\frac{\mathbf{p}}{m_0\gamma}\right]=\lambda n(\mathbf{r},t) \tag{7}$$

and the equation of motion of the fluctuations is found to be

$$\frac{\partial}{\partial t}[\tilde{\mathbf{p}}(\mathbf{r},t)]+\mathbf{v}\cdot\frac{\partial\tilde{\mathbf{p}}(\mathbf{r},t)}{\partial\mathbf{r}}-q\left[\mathbf{E}+\frac{\tilde{\mathbf{p}}\times\mathbf{B}}{\gamma m_0 c}\right]+\nu\tilde{\mathbf{p}}=0 , \tag{8}$$

where $v=\lambda[N_0/n_0-1]$.

It is noticed that the global effects of injecting new plasma into an oscillating plasma are (a) the time-varying plasma density results in a time-varying plasma frequency and (b) and ionization rate introduces an effective damping for the single-fluid momentum [15]. Making the analogy with a mass-spring system, these effects can be easily understood. Since the newly added mass is initially at rest, it slows down the oscillating mass and at the same time changes the spring constant, i.e., the oscillation frequency. The obtained fluid, Eqs. (7) and (8), complemented by Maxwell's equations are used to derive the equation of motion of the longitudinal fluid element displacement in a plasma with a rippled density. The driving force is the ponderomotive force resulting from the beating of two transverse linearly polarized electromagnetic waves.

C. Equation of motion

The equation of motion for a Lagrangian oscillator [20] moving in a one-dimensional cold plasma in the electrostatic limit is now given by

$$\frac{\partial p}{\partial t}=-eE+F_{NL}-\nu p . \tag{9}$$

Here p is the 1D fluctuating part of the fluid element momentum $\tilde{\mathbf{p}}$ [see Eq. (A10)]. The damping term contains the effect of ionization and in addition any other (phenomenological) momentum damping mechanism

(e.g., collisions). The ions are assumed to be immobile. F_{NL} is the ponderomotive force given by [21]

$$F_{NL}=\frac{m_0}{\gamma}c\Delta\omega\frac{\alpha_1\alpha_2}{2}\sin(\Delta k\,x-\Delta\omega\,\tau)\ . \tag{10}$$

Here γ is the Lorentz factor, m_0 the electron rest mass, c the speed of light, and $\alpha_{1,2}$ the quiver velocity of the electrons in the laser fields normalized to the speed of light.

As long as the Lagrangian fluid elements do not cross, the one-dimensional Gaussian law can be integrated immediately to give the electric field, i.e.,

$$E+4\pi e\int_0^{\xi}n_i(x=x_0+\xi')d\xi'\ . \tag{11}$$

In the usual case n_i is uniform ($=n_e$), so one has $E=4\pi n_e\xi$, the simplicity of which accounts for the popularity of the model. Koch and Albritton [22] used the model in a ramp plasma $[N_c(x)=N_0(1+x/L)=N_0(1+x_0/1+x/L)]$ to investigate wave breaking in plasma waves driven by so-called optical resonance. Here we are interested in a rippled plasma [23]

$$n_i=N_0(1+\epsilon\sin k_i x) \tag{12}$$

or, substituting for $x=x_0+\xi$

$$n_i=N_0[1+\epsilon\sin k_i(x_0+\xi)]\ , \tag{13}$$

where ξ is the ripple size. This periodic density ripple is particularly interesting since experimentally it has been observed that such a ripple is easily excited in a tunnel-ionized plasma through stimulated Brillouin scattering, coincidentally with a beat-excited electron plasma wave [18]. The effect of random ripples is not considered but will be the subject of future studies. From Eq. (11) we then obtain for the electric field

$$E=4\pi eN_0\int_0^{\xi}[1+\epsilon\sin k_i(x_0+\xi')]d\xi' \tag{14}$$

or

$$E=4\pi eN_0\left[\xi+\frac{\epsilon}{k_i}(\cos k_i x_0-\cos k_i(x_0+\xi)\right]\ . \tag{15}$$

Using

$$\frac{\partial p}{\partial t}=m_0\gamma^3\frac{\partial v_e}{\partial t} \tag{16}$$

and

$$\frac{\partial\xi}{\partial t}=v_e\ , \tag{17}$$

Eq. (9) becomes

$$\frac{\partial^2\xi}{\partial t^2}+\frac{\nu}{\gamma^2}\frac{\partial\xi}{\partial t}+\frac{\omega_p^2}{\gamma^3}\left[\xi+\frac{\epsilon}{k_i}\cos[k_i x_0-\cos k_i(x_0+\xi)]\right]=\Delta\omega\frac{c}{\gamma^4}\frac{\alpha_1\alpha_2}{2}\sin[\Delta k(x_0+\xi)-\Delta\omega\,t]\ , \tag{18}$$

where

$$\gamma^{-1}=\left[1-\frac{v_e^2+v_\perp^2}{c^2}\right]^{1/2} \tag{19}$$

with $(v_\perp/c)=\alpha_1\alpha_2$, which depends on the laser intensities.

From the dispersion relation for electromagnetic waves in a plasma we also have

$$c\Delta k=c(k_1-k_2)=\Delta\omega\left[1+\frac{\omega_p^2}{2\omega_1\omega_2}\right] \tag{20}$$

and since typically $\omega_1,\omega_2\gg\omega_p$ this reduces to $c\Delta k\approx\Delta\omega$. We now have to distinguish between sweeping the plasma frequency through ionization and/or plasma blowout, and sweeping the driver frequency [8] through, for example, chirping the laser beam. For the former we normalize time with respect to $\Delta\omega^{-1}$, space with respect to Δk^{-1}, and obtain

$$\frac{\partial^2 w}{\partial\tau^2}+\frac{\alpha}{\gamma^2}\frac{\partial w}{\partial\tau}+\frac{\beta^2}{\gamma^3}\left\{w+\epsilon\frac{\Delta k}{k_i}\left[\cos w_0-\cos\left[w_0+\frac{k_i}{\Delta k}w\right]\right]\right\}=\frac{1}{\gamma^4}\frac{\alpha_1\alpha_2}{2}\sin[(w_0+w)-\tau] \tag{21}$$

with $w=\Delta k\xi$, $w_0=k_i x_0$, $\tau=\Delta\omega\,t$, $\alpha=\nu/\Delta\omega$, $\beta=\omega_p/\Delta\omega$, and $\gamma=[1-(w_0/\Delta\omega)^2-\alpha_1\alpha_2]^{-1/2}$. For the latter we normalize time with respect to ω_p^{-1}, space with respect to c/ω_p, and obtain

$$\frac{\partial^2\zeta}{\partial\eta^2}+\frac{\Gamma}{\gamma^2}\frac{\partial\zeta}{\partial\eta}+\frac{1}{\gamma^3}\left[\zeta+\frac{\epsilon}{\kappa}[\cos\kappa w_0-\cos\kappa(w_0+\zeta)]\right]=\frac{\Delta\omega}{\omega_p}\frac{1}{\gamma^4}\frac{\alpha_1\alpha_2}{2}\sin\left[\frac{\Delta\omega}{\Omega_p}(w_0+\zeta)-\frac{\Delta\omega}{\omega_p}\eta\right] \tag{22}$$

with $\zeta=\xi/c/\omega_p$, $w_0=x_0/c/\omega_p$, $\eta=\omega_p\tau$, $\Gamma=\nu/\omega_p$, $\kappa=ck_i/\omega_p$, and $\gamma=[1-(\dot{\zeta})^2-\alpha_1\alpha_2]^{-1/2}$.

The results of numerically solving the equation of motion given by Eqs. (21) and (22) are presented in the next section. Since the obtained results for sweeping ω_p or sweeping $\Delta\omega$ are very similar, we limit the discussion to the case of a time-varying plasma frequency.

III. NUMERICAL RESULTS

In order to capture the full nonlinear complexity of the behavior of the plasma waves, it is necessary to resort to a numerical integration of the relativistic equation of motion for the Lagrangian fluid element as given by Eqs. (21) and (22). Due to the high dimensionality of this parameter space we have limited ourselves to a subspace of experimentally accessible values. In principal the damping rate has contributions due to collisions, Landau damping [21], ionization of the plasma, and mode coupling [23] to slow-phase-velocity plasma waves. As pointed out by Matte and Martin [24] collisional damping is negligible for the case of relatively large driver strengths ($v_{\rm osc}/c$ larger than 0.1) and plasma wave amplitudes. Landau damping is only important when the ratio

of phase velocity of the waves to thermal velocity of the plasma electrons v_ϕ/v_{th} is less than 4. Therefore as a direct damping mechanism for the high-phase-velocity waves it can be neglected. However, mode coupling can establish very efficient transfer [25] between fast and slow electron plasma waves which can couple their energy to the plasma through Landau damping. Its contribution to the damping rate is typically on the order of a few percent. The contribution of the ionization process to the damping depends on the ionization rate which in this paper is assumed to be on the order of $0.01\omega_p$. Therefore the total damping rate is varied within the range $0.01\omega_p - 0.1\omega_p$.

The range of wave-number ratios is determined as follows. One mechanism for generating the density modulation is the generation of ion waves through stimulated Brillouin scattering (SBS). This produces ion waves with wave number $k_i = 2k_0$, where k_0 is the wave number of the laser frequency. If we take the experimental conditions of the experiment of Leemans *et al.* [18], the ratio $k_i/\Delta k$ can be varied from about 19 to 71 by taking different laser line pairs to excite the beat wave. However this ratio can be as low as 2 if one considers the ion wave to be generated through the ion-acoustic decay instability. The ion wave could be present in a partially preionized plasma before the beat wave has grown by using a short high-intensity laser pulse riding on a moderately intense pedestal. The pulse pedestal would generate an ion wave through SBS in the preformed plasma, while the high-intensity pulse would then complete the ionization of the gas and generate a beat wave in the rippled plasma.

We consider for most cases a driver strength limited to $v_{osc}/c = 1$. The detuning ratio $\omega_p/\Delta\omega$ is varied in the range of 0.5–2. We have chosen to vary these two parameters as a function of time while keeping the others constant.

A. Detuning ratio and laser intensity varying with time

It has been suggested that sweeping the plasma frequency [15] or laser frequency [8] in time could result in building up a large-amplitude plasma wave. The idea is to compensate for the relativistic detuning which lowers the plasma frequency by increasing the plasma density, and thereby keeping the driver and plasma wave longer in phase. For the case of an unrippled plasma density we have observed hysteresis loops [8] in plotting the fluid element displacement versus detuning ratio when $\omega_p/\Delta\omega \approx 1.0$ and $\omega_p/\Delta\omega \approx 0.5$ for a range of driver strengths and damping coefficients. An example is shown in Fig. 2 for $v_{osc}/c = 0.2$, $\Gamma = 0.01$. The first loop, around $\omega_p/\Delta\omega \approx 1.0$, is the usual beat-wave excitation which has at exact resonance a secular growth. The second loop, around $\omega_p/\Delta\omega \approx 0.5$, reflects a parametric oscillator excitation process [1] with the pump frequency at about twice the resonance frequency. This mode is seen to grow to saturation at an exponential growth rate for driver strengths large enough to overcome damping.

Aside from this hysteresis effect, half-harmonic generation is observed when the plasma density or the laser intensity are varied as a function of time. We next consider

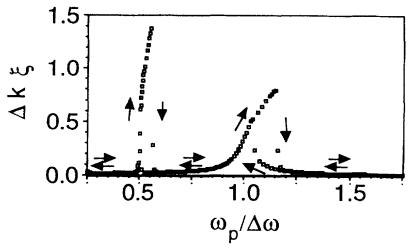

FIG. 2. Detuning curve for a relativistic Lagrangian fluid element for $v_{osc}/c = 0.2$ and $\Gamma = 0.01$ in the absence of a density ripple. The arrows show the existence of hysteresis loops.

in more detail the case of a time-dependent laser intensity. The amplitude of the fluid element excursion was followed as a function of time for a driver strength which had a Gaussian time dependence, i.e.,

$$F = F_0 e^{-(t-t_0/\Delta t)^2} \tag{23}$$

where

$$F_0 = \frac{1}{2}\left[\frac{v_{osc}}{c}\right]^2 \tag{24}$$

corresponds to the peak laser intensity, t_0 is the time at which the laser intensity peaks, and Δt is the laser pulse width. A variety of ratios of the oscillator resonant frequency and the driver frequency were used, as well as a variety of ripple sizes and wave numbers. For very early times the system behaved linearly. The homogeneous solution, oscillating at the natural frequency, was soon dominated by the driven solution. The amplitude increased approximately linearly. At later times the system developed higher harmonics indicating that it had entered the nonlinear regime. The phase-space plot showed an outward spiralling curve, because the driver strength is continuously increasing, and was elliptically shaped due to the harmonic content of the motion.

Then, suddenly, the motion underwent a first bifurcation. The frequency spectrum contained half harmonics $(\frac{1}{2}, \frac{3}{2}, \frac{5}{2})$ while in phase space the limit cycle had split into two loops. For a relatively small ripple size $\epsilon < 0.25$, only one bifurcation was seen, whereas for $0.25 < \epsilon < 0.5$ a second bifurcation could be seen, both cases resulting in an incomplete Feigenbaum tree [6]. Figure 3(a) shows such an incomplete bifurcation tree and the existence of hysteresis for a case where the ripple size $\epsilon = 0.15$, wave-number ratio $k_i/\Delta k = 30$, and detuning parameter $\omega_p/\Delta\omega = 1.7$. For large ripple sizes ($\epsilon \approx 0.75$) the behavior was found to be more complicated [Fig. 3(b)]. For an increasing laser intensity a series of continuous pitchfork bifurcations [26] followed by windows of alternating chaotic and regular motion would occur after the first discontinuous bifurcation. As the intensity reduced the system returned to a periodic motion with period five, underwent a bifurcation to produce period 10 subharmonics, became chaotic again for a narrow range of driver strengths, and eventually followed an inverse period-doubling cascade to return to a regular periodic motion with decreasing amplitude. In these calculations, the damping rate was $\Gamma = 0.03$, the wave-number ratio was

$k_i/\Delta k = 60$, and the peak driver strength was $F = 0.25$.

In Fig. 4(a) a parameter space plot is shown for the driver strength as a function of plasma frequency detuning ratio. We have limited the driver strength to a value corresponding to $v_{osc}/c = 1$ and varied the detuning ratio $\omega_p/\Delta\omega$ from 0.3 to 2.2. As third parameter we have used the ripple amplitude. Two distinctly different regions for the detuning ratio are found. In the absence of the ion ripple, period doubling was only observed around $\omega_p/\Delta\omega \approx 0.5$ in a parameter subspace of $(\omega_p/\Delta\omega, F)$ resembling an Arnold tongue [26]. Lowering the damping rate had the effect of lowering the tip of the "tongue."

In the presence of an ion ripple, it was found that the Arnold-like tongue around $\omega_p/\Delta\omega \approx 0.5$ became slightly broader and the tip of the tongue was also found to extend further down as the ripple strength increased. In addition to this modification of the parametric instability, a new parameter subspace around $\omega_p/\Delta\omega \approx 1.8$ was found in which period doubling occurred for v_{osc}/c varying between 0.1 and 1.

The range of wave-number ratios for which bifurcations occur is found to be limited to $15 < k_i/\Delta k < 130$. As can be seen from the restoring force term in Eq. (23), $k_i/\Delta k$ determines the excursion the fluid element has to make in order to sample the nonlinear restoring force due to the ripple. This explains the lower bound. On the other hand, increasing $k_i/\Delta k$ reduces the electric field contribution of the ripple, and thus the magnitude of the nonlinear term with respect to the linear term, explaining the upper bound. It is also important to note that the detailed nonlinear dynamics of the fluid elements depends on their initial position [i.e., x_0 and w_0 in Eqs. (21) and (22), respectively] in the rippled plasma. This issue will be addressed in the next section.

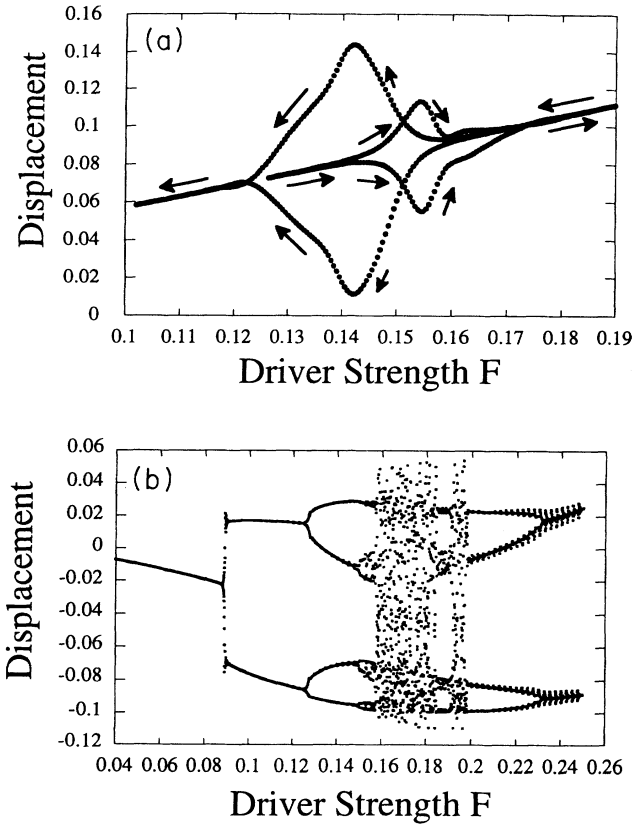

FIG. 3. (a) Bifurcation tree for the relativistic Lagrangian fluid element. The abscissa is the driver strength F and the ordinate is the amplitude of the displacement of the fluid element around the equilibrium position. The driver strength increases linearly with $(v_{osc}/c)_{peak} = 0.7$. The damping rate equals $\Gamma = 0.03\Delta\omega$, ripple size $\epsilon = 0.15$, wave-number ratio $k_i/\Delta k = 30$, and detuning size $\omega_p/\Delta\omega = 1.9$. The arrows show the hysteresis loops existing in conjunction with a bifurcation; (b) same as (a) but with ripple size $\epsilon = 0.75$. Notice a discontinuous jump at $F = 0.09$.

B. Wave breaking

The results obtained have all been based on a Lagrangian-oscillator model. The observed period doubling was associated with the motion of a single oscillator. Therefore if wave breaking due to crossing of the different oscillators occurs before any of the bifurcations occur it would invalidate the above model. Furthermore one needs to know if wave breaking would not prevent one from observing this phenomenon in a laboratory experiment. Since the displacement of the fluid element will contain spatial frequencies at Δk_i, wave breaking will occur when $\Delta k_i \xi > 1$. To verify whether the period-

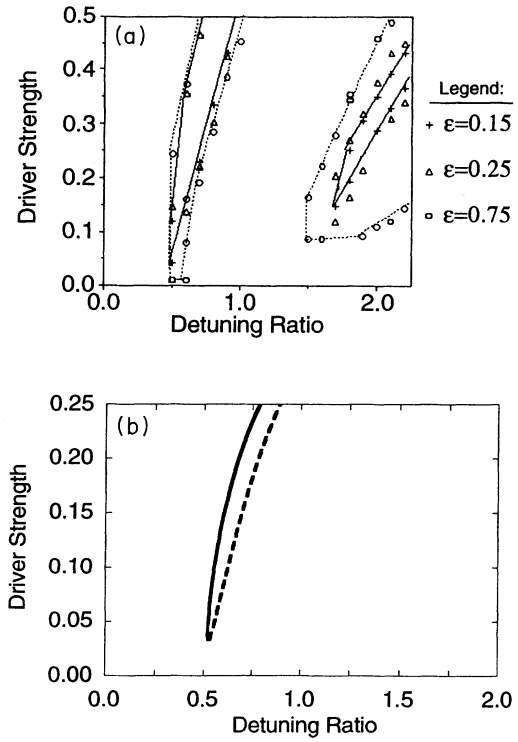

FIG. 4. (a) Parameter space plot of driver strength vs detuning ratio for different ripple sizes ($\epsilon = 0.15$, 0.25, and 0.75) for which the indicated phenomena occurred. Solid lines and dotted lines connect data points with ripple size $\epsilon = 0.15$ and 0.75, respectively; (b) analytically calculated region in parameter space for which the Lagrangian-oscillator equation, in the absence of a ripple, is unstable to half-harmonic perturbations.

doubling route can be completely modelled with the Lagrangian-oscillator model, we followed the motion of many oscillators (up to 1000 per ion wave length) starting out with different equilibrium positions. It was found that wave breaking occurs before the second bifurcation takes place but after the first bifurcation. For example, taking $\epsilon=0.15$, $k_i/\Delta k=60$, $\omega_p/\Delta\omega=1.775$, $\Gamma=0.03$, a first period doubling was observed for $F=0.11$, while wave breaking was seen for $F=0.226$. This clearly limits the validity of our model for describing the period-doubling route in this beat-wave system. Furthermore, one-dimensional models are typically characterized by a higher wave-breaking threshold than two- or three-dimensional models, which could restrict the accessible parameter space even further. This issue needs further theoretical investigation. The origin of this first bifurcation, which occurs before the onset of wave breaking, is analyzed in the next section.

IV. ORIGIN OF THE FIRST BIFURCATION

The analysis is based on a theoretical study by Szemplinska-Stupnicka and Bajkowski [27] on the $\frac{1}{2}$ subharmonic resonance and its transition to chaotic motion in a nonlinear oscillator. The analysis proceeds as follows. First we reduce the model equation of the driven relativistic Lagrangian oscillator to an equivalent driven Mathieu-Duffing equation. After solving for a steady-state solution, oscillating at the driver frequency, the stability against half-harmonic perturbations is analyzed. The resulting equations describe the boundary of the region of $(\Delta\omega/\omega p,F)$ parameter space in which the steady-state solution is unstable against perturbations at half the driver frequency. For completeness we have derived these equations in the general case of nonzero ripple. Only for the case of zero-ripple amplitude, however, have we found an analytical solution. The boundary of this region is in excellent agreement with the Arnold-like tongue, obtained by solving the exact Lagrangian equation using a Runge-Kutta routine.

Steady-state solution of the Lagrangian oscillator

We start from the driven relativistic Lagrangian-oscillator equation [Eq. (21)] which models the behavior of a Lagrangian fluid element moving in a plasma with a density ripple under the influence of the ponderomotive force

$$\ddot{u}+\frac{\alpha}{\gamma^2}\dot{u}+\frac{\beta^2}{\gamma^3}(u+\delta\sin Ku)=-\frac{F}{\gamma^4}\cos(u-\tau)\ . \tag{25}$$

Here $K=k_i/\Delta k$, $u=Kw$, and $\delta=\epsilon/K$, and we have chosen the phase of the electron in the ripple to be $w_0=\pi/2$ in Eq. (21). The choice of this particular phase was made for simplicity. Another choice would result in an additional dc term, which may complicate the mathematical analysis but not affect the physical conclusion. Since we are now interested in threshold u behavior for strong transverse fields, we assume that the longitudinal velocity $\dot{u}$ is small compared to the quiver velocity $v_{\rm osc}$ so that the Lorentz factor γ can be approximated as

$$\gamma\approx\left[1-\left[\frac{v_{\rm osc}}{c}\right]^2\right]^{-1/2}=\Gamma\ . \tag{26}$$

Expanding the cosine function in Eq. (25) and using Eq. (26) we then obtain

$$\ddot{u}+\alpha_1(t)\dot{u}+[\alpha_2(t)+\alpha_3(t)\sin\tau]u+\alpha_4(t)\delta\sin Ku=-\alpha_3(t)\cos\tau\ , \tag{27}$$

where

$$\alpha_1(t)=\frac{\alpha}{\Gamma^2}\ ,\quad \alpha_2(t)=\frac{\beta^2}{\Gamma^3}\ ,\quad \alpha_3(t)=\frac{F}{\Gamma^4}\ . \tag{28}$$

We now write $v=Ku$ so that Eq. (28) becomes

$$\ddot{v}+\alpha_1\dot{v}+(\alpha_2+\alpha_3\sin\tau)v+\alpha_2K\delta\sin v=-K\alpha_3\cos\tau \tag{29}$$

and will look for a steady-state solution of Eq. (29) of the form

$$v=v_0(t)=C_0+C_1\cos(\tau+\theta)\ . \tag{30}$$

Substituting Eq. (30) into Eq. (29), using the identities

$$\cos(a\cos\tau)=2\sum_{n=0}^{\infty}(-1)^nJ_{2n}(a)\cos(2n\tau)-J_0(a)\ , \tag{31}$$

$$\sin(a\cos\tau)=2\sum_{n=0}^{\infty}(-1)^nJ_{2n+1}(a)\cos[(2n+1)\tau] \tag{32}$$

and grouping terms oscillating at the same frequency and phase, we find

dc term,

$$\alpha_2C_0-\tfrac{1}{2}\alpha_3C_1\sin\theta+\alpha_2\delta\sin C_0J_0(C_1)=0\ ; \tag{33}$$

$\cos(\tau+\theta)$ term,

$$-C_1+\alpha_2C_1-\alpha_3C_0\sin\theta+2\alpha_2\delta\cos C_0J_1(C_1)=-K\alpha_3\cos\theta; \tag{34}$$

$\sin(\tau+\theta)$ term, $-\alpha_1C_1+\alpha_3C_0\cos\theta=-K\alpha_3\sin\theta$. (35)

From Eqs. (33)–(35) one can then find C_0, C_1, and θ to calculate the steady-state solution v_0.

We now perturb v_0, i.e., $v=v_0+\delta v$, and substitute this into Eq. (29)

$$\delta\ddot{v}+\ddot{v}_0+\alpha_1(\dot{v}_0+\delta\dot{v})+(\alpha_2+\alpha_3\sin\tau)(y_0+\delta v)+\alpha_2\delta\sin(v_0+\delta v)=-K\alpha_3\cos\tau\ . \tag{36}$$

Assuming that the amplitude of the perturbation δv is small such that $\cos\delta v\approx1$ and $\sin\delta v\approx\delta v$, and realizing that v_0 is a solution of Eq. (29) we find

$$\delta\ddot{v}+\alpha_1\delta\dot{v}+(\alpha_2+\alpha_3\sin\tau+\alpha_2\delta\cos v_0)\delta v=0\ . \tag{37}$$

But $v_0=C_0+C_1\cos(vt+\theta)$, and hence Eq. (13) becomes

$$\delta\ddot{v}+\alpha_1\delta\dot{v}+\{\alpha_2+\alpha_3\sin\tau+\alpha_2\delta\cos[C_0+C_1\cos(\tau+\theta)]\}\delta v=0\ . \tag{38}$$

Using the identities from Eqs. (31) we can rewrite Eq. (38) as

$$\delta\ddot{v}+\alpha_1\delta\dot{v}+\left\{\alpha_2[1+\delta J_0(C_1)]+\alpha_3\sin\tau-2\alpha_2\delta\sin C_0\sum_{n=0}^{\infty}(-1)^n J_{2n+1}(C_1)\cos[(2n+1)(\tau+\theta)]\right.$$
$$\left.+\alpha_2\delta\cos C_0\left[2\sum_{n=1}^{\infty}(-1)^n J_{2n}(C_1)\cos[2n(\tau+\theta)]\right]\right\}\delta v=0\ . \tag{39}$$

Rewriting $\sin\tau$ as $\sin\tau=\sin(\tau+\theta)\cos\theta-\cos(\tau+\theta)\sin\theta$ and grouping terms, Eq. (39) becomes

$$\delta\ddot{v}+\alpha_1\delta\dot{v}+\left\{\delta_1+\alpha_3\cos\theta\sin(\tau+\theta)-[\alpha_3\sin\theta+2\alpha_2\delta\sin C_0 J_1(C_1)]\cos(\tau+\theta)\right.$$
$$\left.+2\delta\alpha_2\sum_{n=2}^{\infty}a_n(-1)^n\cos[n(\tau+\theta)]\right\}\delta v=0\ , \tag{40}$$

where $\delta_1=\alpha_2[1+\delta J_0(C_1)]$ and a_n is equal to $-\sin C_0(\cos C_0)$ for n odd (even). Equation (40) is now in the form of Mathieu's equation which has been studied extensively. To study the stability of the Lagrangian oscillator equation [Eq. (25)] we now concentrate on the behavior of the perturbation δv with time. According to the results of studies by Hayashi and Abramowitz and Stegun [28] and Szemplinska-Stupnicka and Bajkowski [27] of the Mathieu equation, the lowest-order unstable region occurs at a frequency close to

$$\sqrt{\delta_1}\cong\tfrac{1}{2}\ , \tag{41}$$

and we therefore assume as approximate solution for the perturbation

$$\delta v(\tau)=e^{\epsilon\tau}b_{1/2}\cos(\tfrac{1}{2}\tau+\phi)\ , \tag{42}$$

where $\epsilon>0$ for an unstable region and ϕ is the phase with respect to the driver frequency. At the stability limit $\epsilon=0$ and hence

$$\delta v(\tau)=b_{1/2}\cos(\tfrac{1}{2}\tau+\phi)\ . \tag{43}$$

Substituting Eq. (43) into Eq. (40) and grouping terms in cosine and sine we find the set of equations

$$G\cos\theta\cos2\phi+\left[\frac{\alpha_3}{2}+G\sin\theta\right]\sin2\phi=(\delta_1-\tfrac{1}{4})\ ,$$
$$\left[\frac{\alpha_3}{2}-G\sin\theta\right]\cos2\phi+G\cos\theta\sin2\phi=-\frac{\alpha_1}{2}\ , \tag{44}$$

where

$$G=\alpha_2\delta\sin C_0 J_0(C_1) \tag{45}$$

and C_0, C_1, and θ are the steady-state solutions of Eq. (29). Solving Eq. (45) and using the fact that $\sin2\phi$ and $\cos2\phi$ are not independent, we arrive at

$$\frac{(g_1g_5+g_3g_4)^2+(g_1g_3+g_2g_4)^2}{(g_3^2-g_2g_5)^2}=1 \tag{46}$$

where

$$g_1=\delta_1-\tfrac{1}{4}\ ,g_2=\frac{\alpha_3}{2}+G\sin\theta\ ,$$
$$g_3=G\cos\theta\ ,\quad g_4=\frac{\alpha_1}{2}\ ,g_5=\frac{\alpha_3}{2}-G\sin\theta\ . \tag{47}$$

The boundaries of the unstable regions can then be determined by solving the coupled nonlinear equations Eqs. (33)–(35) and (46) and (47) using numerical techniques. To illustrate the model we will analytically solve the case of zero-ripple amplitude, i.e., $\delta=0$. The set of equations (33)–(35) then simplifies to

$$\alpha_3C_0=\tfrac{1}{2}\alpha_3C_1\sin\theta\ ,$$
$$C_1(1-\alpha_2)+\alpha_3C_0\sin\theta=K\alpha_3\cos\theta\ , \tag{48}$$
$$\alpha_1C_1-\alpha_3C_0\cos\theta=K\alpha_3\sin\theta$$

from which one can obtain the amplitudes of C_0, C_1, and θ as a function of the ripple amplitude δ, the wave number of the ripple K, the driver strength F, and the detuning ratio β

$$C_0=\frac{K\alpha_1\alpha_3^2}{2\alpha_2[\alpha_1^2+(1-\alpha_2)^2]+\alpha_3^2(1-\alpha_2)}\ , \tag{49}$$

$$C_1^2=-\frac{2\alpha_2C_0(C_0^2+K^2)}{C_0(1-\alpha_2)-\alpha_1K}\ , \tag{50}$$

$$\sin\theta=\frac{2\alpha_2C_0}{\alpha_3C_1}\ . \tag{51}$$

From Eq. (45) we see that $G=0$ for $\delta=0$ and hence Eq. (46) reduces to

$$[2(\alpha_2-\tfrac{1}{4})]^2+\alpha_1^2=\alpha_3^2\ . \tag{52}$$

Using Eq. (28) we finally obtain

$$\frac{\omega_p}{\Delta\omega}=\Gamma^{3/2}\left\{\tfrac{1}{4}\pm\tfrac{1}{2}\left[\left[\frac{F}{\Gamma^4}\right]^2-\left[\frac{\alpha}{\Gamma^2}\right]^2\right]^{1/2}\right\}^{1/2}\ , \tag{53}$$

which describes the boundary of the parameter region for which the steady-state solution of the oscillator is unstable to half-harmonic perturbations. Here, from Eq. (26),

$\Gamma=(1-2F)^{-1/2}$. The boundary of this unstable region is shown in Fig. 4(b). We also note that the existence of a half-harmonic resonance is consistent with the discontinuous first bifurcation observed in the numerical results. To assess whether even this first bifurcation could survive in a "real" plasma we resorted to particle-in-cell (PIC) simulations, which are the subject of Sec. V.

V. PIC-Code Results

The object of the particle-in-cell simulations was to verify that a period doubling (and if possible a route to chaos) can occur in the generation of relativistic plasma waves through collinear optical mixing even when other one-dimensional competing effects are included. Some of the competing effects are Raman backscatter, electron heating, parametric decay of the Raman backscatter wave, mode coupling, etc.

In the simulations, the laser is incident from the left along the x axis and is polarized along z. To reduce the amount of computing time we have kept the ions immobile. To model the density ripple the electrons and fixed ion background were initialized at time $t=0$ with a sinusoidal ripple.

Frequencies are normalized to the background (excluding the ripple) plasma frequency $\omega_p 0$. Distances are normalized to the collisionless skin depth $c/\omega_p 0$. For display purposes the wave numbers are given in units of mode number, N_{mode}, the number of wavelengths of a given sinusoidal mode that will fit within the simulation box $kxN_{\text{mode}}=kL/2\pi$, where L is the length of the box, in this case $210c/\omega_{p0}$, chosen to accommodate 20 waves with wavelength $2\pi/\Delta k$.

Three different simulations have been performed: (i) rippled ion background at $t=0$, (ii) no density ripple at $t=0$ but with plasma temperature low enough so that the short-wavelength plasma modes produced through backward SRS are not Landau damped and hence will produce a rippled plasma, and (iii) no density ripple at $t=0$ and high plasma temperature so that the short-wavelength plasma modes are Landau damped. We have chosen to use parameters in the PIC-simulation which have shown one bifurcation in the analytic model. The plasma frequency is equal to one in simulation units while the two laser frequencies are chosen to give a detuning ratio $\omega_p/\Delta\omega=1.7{:}\omega_1=5$ and $\omega_2=4.411$ in ω_p units. In simulation units the dispersion relation for light waves in a plasma is given by

$$\omega_{1,2}^2=1+k_{1,2}^2 \ . \tag{54}$$

The chosen laser frequencies give a plasma wave number $\Delta k=(24)^{1/2}-[(4.411)^2-1]^{1/2}=0.602$. The ripple wave number is taken to be $k_i/\Delta k=30$ and the ripple size $\epsilon=0.2$. The peak laser intensity results in a normalized quiver velocity $v_{\text{osc}}/c=0.6$. The simulations were carried out in an essentially one-dimensional system on a 2×6000 grid of normalized dimension 1×210 (in c/ω_p units). This implies that the system can contain 20 plasma wavelengths oscillating at the beat frequency. A total of 120 000 particles were used (10 particles per cell). The simulation was set up to record plasma parameters every $\Delta(\omega_p T)=25$ (every 1000 time steps) except for the ω spectrum which was recorded every 2000 time steps.

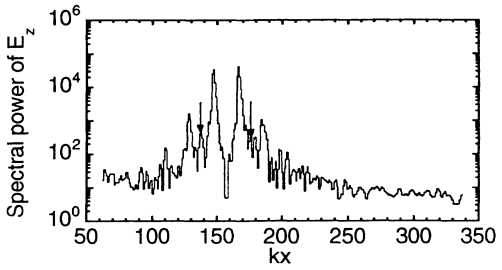

FIG. 5. k spectrum of the transverse electric field E_z as obtained from the WAVE simulation code at time step $T=150$. The left and right arrows denote the location of the half-harmonic at $k_2-\frac{1}{2}(k_1-k_2)$ and at $k_1+\frac{1}{2}(k_1-k_2)$, respectively.

The main diagnostic consists of the k spectrum of the transverse electric (E_z) field. Indeed, if spatial period doubling occurs in conjunction with temporal period doubling of the kind observed in the Lagrangian fluid model, the phase matching condition is satisfied for the laser frequencies to scatter from these subharmonics of the plasma wave. The k spectrum of the transverse field should show Stokes and anti-Stokes lines of the laser frequencies which are shifted by subharmonics of the beat frequency.

At $T=0$ the simulation was initialized with the above parameters. At $T=150$, as shown in Fig. 5, the k spectrum of the transverse electric field E_z contains Stokes and anti-Stokes lines shifted by subharmonics of the beat frequency. Since these features will only show up in the electromagnetic spectrum when the phase matching conditions are met, this implies that the plasma wave form contains subharmonics both in space and in time.

In the numerical model we have found that a range existed for density modulation wavelengths $k_i/\Delta k$ had to be between 15 and 130 to observe period doubling. For the simulation parameters, plasma waves produced through Raman scattering or ion waves produced through SBS or the ion acoustic decay instability would result in density modulation with wave-number ratio between 2 and 10. In order to verify that the observed subharmonics are caused by the short-wavelength density modulations due to the imposed ion ripple, we have performed two null tests. While in both tests the initial ripple is absent, the thermal electron velocity at $T=0$ was set equal to $0.025c$ in the first test while in the second test it was set to $0.15c$. This higher plasma temperature resulted in Landau damping of the slow-phase-velocity plasma waves, and no period doubling was observed. While SRS did modulate the density in the lower temperature case, the k was too low and no period doubling was observed here consistent with the analytic results.

VI. CONCLUSION

A numerical study has been performed of the nonlinear dynamics of the generation of a plasma wave through col-

linear optical mixing in a spatially modulated plasma with time-varying parameters. The numerical study was based upon the Lagrangian equation of motion for a fluid element moving under the influence of an intense laser pulse in the presence of an ion density modulation. The choice for working in a Lagrangian frame arose from the need to treat rigorously the relativistic mass increase of the fluid electrons for large laser intensities. It was shown that resorting to the weakly relativistic approximation in an Eulerian frame leads to the erroneous conclusion that beat excitation of plasma waves can be modelled with a Duffing equation. The two nonlinear phenomena on which we have concentrated are bistability with the associated hysteresis loops and period doubling with the possibility of evolving into chaos. The parameters which determine the amplitude of the plasma wave were chosen to be the laser intensity, the plasma density, the damping rate, the wavelength, and amplitude of the density modulation.

The obtained model equation was solved numerically because the commonly used slowly varying amplitude approximation precludes one from observing subharmonics in the frequency spectrum of the wave amplitude.

When the laser intensity or the plasma density was varied in time, the amplitude of the plasma wave as a function of either of these parameters showed hysteresis loops. Furthermore, in the absence of a ripple, an Arnold tonguelike region was found for detuning ratios around $\Delta\omega/\omega_p \approx 0.5$, in which the motion of the fluid element shows spectral components at subharmonic frequencies of the driver frequency. In the presence of a short-wavelength density modulation, a second Arnold tonguelike region became accessible around $\Delta\omega/\omega_p \approx 1.8$. For relatively small-amplitude density modulations the fluid element oscillations underwent bifurcations, leading to subharmonics in the spectrum, followed by inverse bifurcations which led to a regular periodic motion oscillating at the driver frequency. For large density modulations a cascade of bifurcations occurred followed by a transition to chaos and consecutive periodic windows.

By following many Lagrangian oscillators simultaneously it was found that wave breaking occurred before the second period doubling, thereby limiting the validity of the Lagrangian-oscillator model. The origin of the first bifurcation was then linked to the stability of an equivalent generalized Mathieu equation to $\frac{1}{2}$ subharmonic resonances.

Fully relativistic PIC-code simulations were carried out to investigate further the bifurcation behavior. Through analysis of the k spectrum of the transverse electric field E_z and magnetic field B_y it was found that spectral components exist with k-space separations of half the k-space difference between the two drivers $(k_1 - k_2)$. Since these features only show up in the electromagnetic spectrum when the phase-matching conditions are met, we conclude that this spatial difference period doubling must occur in conjunction with temporal beat period doubling. It needs to be mentioned however that for these simulations a very extensive amount of computer time was needed and the ions had to be kept immobile. Future work should address the issue of self-consistent density modulation caused by finite mass ions and the resulting competition between this possible path to turbulence and phenomena such as Langmuir collapse.

ACKNOWLEDGMENTS

We acknowledge useful discussions with Dr. P. K. Kaw and Dr. J. M. Dawson. This work was supported by DOE Contract No. DE-AS03-ER 40120 and DOE Grant No. DE-FG 03-88 ER 40474.

APPENDIX

To obtain the fluid equations in an ionizing, relativistic plasma we now proceed with the Vlasov equation for a one-particle distribution function to which a source term $S(\mathbf{r},\mathbf{p},t)$ has been added to model the time-varying plasma density

$$\frac{\partial f}{\partial t} + \frac{\mathbf{p}}{\gamma m_0}\cdot\frac{\partial f}{\partial \mathbf{r}} + q\left[\mathbf{E} + \frac{\mathbf{p}\times\mathbf{B}}{\gamma m_0 c}\right]\cdot\frac{\partial f}{\partial \mathbf{p}} = S(\mathbf{r},\mathbf{p},t)\ , \tag{A1}$$

$$\dot{\mathbf{p}} = q\left[\mathbf{E} + \frac{\mathbf{v}\times\mathbf{B}}{c}\right] = \frac{d}{dt}(m_0\gamma v)\ , \tag{A2}$$

$$\dot{\mathbf{r}} = \mathbf{v},\quad \mathbf{v} = \frac{\mathbf{p}}{\gamma m_0}\ . \tag{A3}$$

where m_0 and q are, respectively, the rest mass and charge of an electron, γ is the Lorentz factor, f is the one-particle distribution function, and $\mathbf{E}$ and $\mathbf{B}$ are the electric and magnetic fields. The source term for a tunnel-ionized plasma is given by Eq. (6). We assume the plasma to be perfectly cold, i.e.,

$$f(\mathbf{r},\mathbf{P},t) = \tilde{f}(\mathbf{r},t)\delta(\mathbf{P}-\mathbf{p})\ , \tag{A4}$$

where $\mathbf{P}=\mathbf{P}(\mathbf{r},t)$ is the momentum of a particular fluid element and $\mathbf{p}=\mathbf{p}(\mathbf{r},t)$ is the momentum averaged over all fluid elements. To obtain fluid equations we take moments of Eq. (A1). The mean density and velocity are, respectively, defined as

$$n = \int_{-\infty}^{+\infty} d^3p\, f \tag{A5}$$

and

$$v = \frac{1}{n}\int_{-\infty}^{+\infty} d^3p \frac{f(\mathbf{r},\mathbf{P},t)}{m_0\gamma}\ . \tag{A6}$$

Denoting the fluctuating density by $\tilde{n}=\tilde{n}(\mathbf{r},t)$ and the time-dependent background electron density by $n_0=n_0(\mathbf{r},t)$, we write the total electron density as $n=n(\mathbf{r},t)=n_0(\mathbf{r},t)+\tilde{n}(\mathbf{r},t)$. Taking the zeroth-order moment and using Eqs. (A5) and (A6) we obtain the continuity equation with the inclusion of a source term:

$$\frac{\partial n}{\partial t} + \nabla\cdot\left[n(\mathbf{r},t)\frac{\mathbf{p}}{m_0\gamma}\right] = \lambda(t)(N_0 - n_0)\ . \tag{A7}$$

Note that since the newly born electrons start out at rest there is no contribution of $\tilde{n}(t)$ in the right-hand side of Eq. (A7).

Taking the first-order moment we find

$$\frac{\partial}{\partial t}(\mathbf{p}n)+\frac{\partial}{\partial \mathbf{r}}\left[\frac{\mathbf{p}^2}{\gamma m_0}n(\mathbf{r},t)\right]-q\left[\mathbf{E}+\frac{\mathbf{p}\times\mathbf{B}}{\gamma m_0 c}\right]n=0\ . \tag{A8}$$

But the first term in Eq. (A8) can be written out as

$$\frac{\partial}{\partial t}(\mathbf{p}n)=n\frac{\partial \mathbf{p}}{\partial t}+\mathbf{p}\frac{\partial n}{\partial t}\ . \tag{A9}$$

Multiplying Eq. (A7) by $\mathbf{p}$ and subtracting it from Eq. (A8) we obtain as an equation of motion

$$\frac{\partial \mathbf{p}}{\partial t}+\mathbf{v}\frac{\partial \mathbf{p}}{\partial \mathbf{r}}-q\left[\mathbf{E}+\frac{\mathbf{p}\times\mathbf{B}}{\gamma m_0 c}\right]+\lambda\mathbf{p}\frac{(N_0-n_0)}{n}=0\ , \tag{A10}$$

where we used the definitions of $\dot{\mathbf{r}}$ and $\mathbf{v}$ given in Eq. (A3). The equation of motion for the momentum fluctuations $\tilde{\mathbf{p}}$ is then given by

$$\frac{\partial \tilde{\mathbf{p}}}{\partial t}+\mathbf{v}\frac{\partial \tilde{\mathbf{p}}}{\partial \mathbf{r}}-q\left[\mathbf{E}+\frac{\tilde{\mathbf{p}}\times\mathbf{B}}{\gamma m_0 c}\right]+\lambda\tilde{\mathbf{p}}(N_0/n_0-1)=0\ . \tag{A10'}$$

*Present address: Lawrence Berkeley Laboratory, Berkeley, CA 94720.

[1] M. N. Rosenbluth and C. S. Liu, Phys. Rev. Lett. **29**, 701 (1972).

[2] T. Tajima and J. M. Dawson, Phys. Rev. Lett. **43**, 267 (1979).

[3] D. W. Forslund, J. M. Kindel, and E. L. Lindman, Phys. Fluids **18**, 1002 (1975), and references therein; C. J. Walsh *et al.*, Phys. Rev. Lett. **53**, 1445 (1984); H. A. Rose, D. F. Dubois, and B. Bezzerides, *ibid.* **58**, 2547 (1987); W. P. Leemans *et al.*, *ibid.* **67**, 1434 (1991).

[4] C. M. Tang, P. Sprangle, and R. N. Sudan, Phys. Fluids **28**, 1974 (1985); W. Horton and T. Tajima, Phys. Rev. A **31**, 3937 (1985).

[5] M. J. Feigenbaum, J. Stat. Phys. **19**,(1), 25 (1978).

[6] M. Bier and C. Bountis, Phys. Lett. **104A**, 239 (1984).

[7] R. L. Morse and C. W. Nielson, Phys. Fluids **14**, 830 (1971).

[8] J. X. Ma and Z. Z. Xu, J. Appl. Phys. **65**, 9 (1989).

[9] J. T. Mendonça, J. Plasma Phys. **34**, 115 (1985).

[10] G. Duffing, *Erzwungene Schwingungen bei Veranderlicher Eigenfrequenz* (Vieweg, Braunschweig, 1918).

[11] P. Holmes and D. Rand, J. Sound Vib. **44**, 237 (1976); B. Huberman and J. P. Crutchfield, Phys. Rev. Lett. **43**, 1743 (1979).

[12] W. B. Mori, IEEE Trans. Plasma Sci. **5**, 88 (1987).

[13] C. J. McKinstrie and D. W. Forslund, Phys. Fluids **30**, 904 (1987).

[14] W. P. Leemans and C. Joshi, in *Nonlinear and Relativistic Effects in Plasmas,* Research Trends in Physics, edited by V. Stefan (AIP, New York, 1992), pp. 35–42.

[15] J. P. Matte, F. Martin, N. A. Ebrahim, P. Brodeur, and H. Pepin, IEEE Trans. Plasma Sci. **2**, 15 (1987).

[16] C. E. Max, Phys. Fluids **19**, 74 (1976); P. K. Kaw, G. Schmidt, and T. Wilcox, *ibid.* **16**, 1522 (1973); K. Estabrook, W. L. Kruer, and D. S. Bailey, *ibid.* **28**, 19 (1985); V. K. Tripathi and L. A. Pitale, J. Appl. Phys. **48**, 3288 (1977); B. I. Cohen and C. E. Max, Phys. Fluids **30**, 1115 (1979).

[17] N. Krall and A. W. Trivelpiece, *Principles of Plasma Physics* (McGraw-Hill, New York, 1973).

[18] W. P. Leemans, C. E. Clayton, W. B. Mori, K. A. Marsh, A. Dyson, and C. Joshi, Phys. Rev. Lett. **68**, 321 (1992).

[19] L. V. Keldysh, Zh. Eksp. Teor. Fiz. **47**, 1945 (1964) [Sov. Phys. JETP **20**, 1307 (1965)]

[20] J. M. Dawson, Phys. Rev. **113**, 383 (1959); R. C. Davidson and P. C. Schram, Nucl. Fusion 8,183 (1968).

[21] F. F. Chen, *Introduction to Plasma Physics and Controlled Fusion,* 2nd ed. (Plenum, New York, 1984).

[22] P. Koch and J. Albritton, Phys. Rev. Lett. **32**, 1420 (1974).

[23] C. B. Darrow, D. Umstadter, T. Katsouleas, W. B. Mori, C. E. Clayton, and C. Joshi, Phys. Rev. Lett. **56**, 2629 (1986).

[24] J. P. Matte and F. Martin, Plasma Phys. Controlled Fusion **30**, 395 (1988).

[25] W. Kruer, Phys. Fluids **15**, 2423 (1972); W. L. Kruer and J. M. Dawson, Phys. Rev. Lett. **25**, 1174 (1970).

[26] F. C. Moon, *Chaotic Vibrations* (Wiley, New York, 1987).

[27] W. Szemplinska-Stupnicka and J. Bajkowski, Int. J. Non-Linear Mech. **21**, 401 (1986).

[28] C. Hayashi, *Nonlinear Oscillations in Physical Systems* (McGraw-Hill, New York 1964); *Handbook of Mathematical Functions,* edited by M. Abramowitz and I. A. Stegun (Dover, New York, 1971).